Durham University

Durham Research Online

Deposited in DRO:

19 July 2018

Version of attached file:

Accepted Version

Peer-review status of attached file:

Peer-reviewed

Citation for published item:

Wang, Z. and Huang, S. L. and Wang, S. and Wang, Q. and Zhao, W. (2018) 'Development of a new EMAT for multi-helical SH guided waves based on magnetostrictive effect.', in 2018 IEEE International Instrumentation and Measurement Technology Conference (I2MTC) : 14-17 May 2018, Houston, Texas, USA ; proceedings. Piscataway: IEEE, pp. 1279-1284.

Further information on publisher's website:

https://doi.org/10.1109/I2MTC.2018.8409576

Publisher's copyright statement:

© 2018 IEEE. Personal use of this material is permitted. Permission from IEEE must be obtained for all other uses, in any current or future media, including reprinting/republishing this material for advertising or promotional purposes, creating new collective works, for resale or redistribution to servers or lists, or reuse of any copyrighted component of this work in other works.

Additional information:

Use policy

The full-text may be used and/or reproduced, and given to third parties in any format or medium, without prior permission or charge, for personal research or study, educational, or not-for-profit purposes provided that:

- a full bibliographic reference is made to the original source
- a link is made to the metadata record in DRO
- the full-text is not changed in any way

The full-text must not be sold in any format or medium without the formal permission of the copyright holders.

Please consult the full DRO policy for further details.

Durham University Library, Stockton Road, Durham DH1 3LY, United Kingdom
Tel : +44 (0)191 334 3042 | Fax : +44 (0)191 334 2971
https://dro.dur.ac.uk

Development of a new EMAT for multi-helical SH guided waves based on magnetostrictive effect

[1]Zhe Wang, [1]Songling Huang, *IEEE Senior Member*, [1]Shen Wang,
[2]Qing Wang, *IEEE Senior Member*, [1]Wei Zhao
[1]State Key Laboratory of Power System, Department of Electrical Engineering, Tsinghua University, Beijing, China,
Email: huangsling@mail.tsinghua.edu.cn
[2]School of Engineering and Computing Sciences, Durham University, Durham, UK

***Abstract*—Electromagnetic acoustic transducers (EMATs) have the advantage of non-contact and have been widely used in nondestructive testing (NDT). However, the propagation of the guided wave generated by present transducers is either concentrated with narrow beam directivity or omni-directional with disperse energy. To overcome these disadvantages, a new EMAT is proposed to generate multi-helical shear horizontal (MHSH) guided waves. The waves can propagate in multiple helical angles within a certain range while the energy is still concentrated. In this paper, the excitation and reception process of the guided wave are modeled based on the magnetostrictive effect, and then Finite Element Method (FEM) is applied to confirm the models and to further study the wave radiation pattern. A series of experiment are carried out to evaluate the performance of the proposed EMAT. Finally, the influences of two key design parameters on the beam divergence angle are discussed.**

***Index Terms*—Electromagnetic Acoustic Transducer, Multi-helical Guided Wave, Magnetostrictive Effect, Parameter Analysis**

I. Introduction

Nondestructive testing (NDT) is commonly used for pipe detection, including guided wave detection, eddy current testing and magnetic flux leakage testing. Guided wave can propagate a long distance with low attenuation and has been widely used for rapid defect inspection in pipes [1–4]. Both the piezoelectric transducer and electromagnetic acoustic transducer (EMAT) can generate various modes of guided waves. However, the latter one has the noncontact nature which extends its application.

Among the modes of guided wave, the shear horizontal (SH) guided wave has only one component of displacement. What's more, it is easily generated by EMAT. For plate inspection, researchers have designed beam-focused SH wave transducer [5] and omni-directional SH wave transducer [6]. For pipe inspection, circumferential SH (CSH) guided wave which propagates in the circumferential direction of pipe is applied. CSH wave was initially regarded as SH wave in plate [7], until Xiaoliang Zhao and Joseph L. Rose [8] numerically solved its dispersion curve. They also analyzed the stress wave structure and displacement wave structure. Wei Luo *et al.* [9] arranged the magnetostrictive sensor on the outside wall of the pipe and generated CSH wave in pipe with defects of different depths and lengths. Furtherly, the interaction of CSH wave with defects was simulated in three-dimensional modeling [10]. The CSH wave is sensitive to the axial crack of the pipe, however, it can only detect the defect in the circumference where the transducers is located. The transducers must move along the pipe to complete the inspection.

The helical SH (HSH) guided wave propagating spirally along a hollow cylinder can detect the pipe of long distantance with the transducers in situ. It is used to detect the axial and circumferential defects on the pipe at the same time. Hoe Woong Kim *et al.* [11] succeeded in generating HSH guided wave propagating in helical way by using transducers composed of segmented magnetostrictive patches. Furthermore, they designed a new transducer structure comprising permanent magnets, a figure-of-eight coil and magnetostrictive patches [12]. This transducer generated HSH waves in a wide helical direction and the energy was mainly concentrated in the circumferential direction of the pipe. However, the former transducer have narrow beam directivity. The latter transducer is lack of wave mode control and is nearly omni-directional leading to quite disperse energy.

To promote research into the HSH wave and its transduction mechanism, a new transducer for multi-helical shear horizontal (MHSH) guided waves based on magnetostrictive effect is designed and analyzed in this paper. The transducer can generate MHSH waves in a certain range of helical angle. The energy of waves is still concentrated. Besides, the size of this transducer is ratherly small and the generated guided wave would cover the region of inspection with fewer transducers.

The research is organized as follows. Section II gives the theoretical analysis. In Section III, the design of the new EMAT is described. In Section IV, the complete magnetostrictive model is established. It is simulated by the Finite Element Method (FEM) which also analyzes the wave radiation pattern. In Section V, relevant experiments are carried out to verify the transducer. Meanwhile, two important parameters of central radius and central angel are studied in both simulations and experiments. Section VI presents concluding remarks.

II. Theoretical Analysis

The theory of guided wave in the plate structure has been studied earlier than that of pipe structure. Due to the similarity of the pipe and the plate, the pipe can be approximated as an unwrapped flat plate when the diameter is much larger than the wall thickness and the wavelength is comparable to the wall thickness [13]. The wave velocity of MHSH wave in

pipe traveling along helical line is close to that of SH wave in plates. The difference of wave velocities can be ignored.

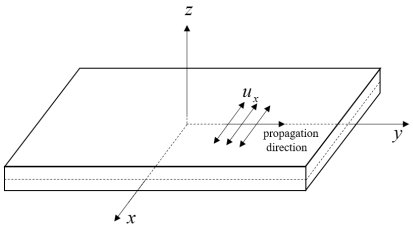

Fig. 1. Displacement component of equivalent SH wave in plate

Fig.1 shows the expanded plane of a pipe. For SH wave, it has only one displacement component which is parallel to x axis and independent of z axis. Based on Navier equation, the displacement is expressed as

$$\frac{\partial^2 u_x}{\partial y^2} + \frac{\partial^2 u_x}{\partial z^2} = \frac{1}{c_T^2}\frac{\partial^2 u_x}{\partial t^2} \tag{1}$$

where, u_x is the displacement component, c_T is the volecity of transverse wave. Combined with boundary conditions $\tau_{yz}|_{z=\pm h} = 0$, the dispersion equation can be concluded:

$$c_p(fd) = 2c_T \frac{fd}{\sqrt{4(fd)^2 - (nc_T)^2}} \tag{2}$$

where, c_p is the phase velocity, f is the frequency of guided wave, d is the thickness of plate, and

$$\begin{aligned} n &\in \{0, 2, 4 \cdots\} \quad Symmetric\ mode \\ n &\in \{1, 3, 5 \cdots\} \quad Antisymmetric\ mode \end{aligned} \tag{3}$$

In terms of the transduction principle, the guided wave is generated mainly by the magnetostrictive effect which occurs only in the ferromagnetic material. The phenomenon of deformation caused by the magnetization is called magnetostrictive effect. The inverse process is known as the inverse magnetostrictive effect. Because of the nonlinear properties of magnetization in ferromagnetic materials and the difficulties of carrying out the corresponding experiments, the magnetostrictive effect has not yet been fully explored.

The theory holds that many small magnetic domains exist in the ferromagnetic material. Without external magnetic field, the directions of these small magnetic domains are random and the magnetic fields generated by each other offset. Under the static magnetic field, the magnetic domains rotate to the direction of the external magnetic field, leading to the tiny deformation of the material. Under dynamic magnetic field, it generates vibration and then forms the ultrasonic wave. Usually a static bias magnetic field and a small dynamic magnetic field are combined to generate the guided wave. The former one provides the operating point and the latter one supplies the perturbation.

III. Design of the New EMAT

In order to overcome the disadvantages of the narrow beam directivity and disperse energy, a new EMAT for MHSH waves is proposed. Its structure is illustrated in Fig. 2. It looks like a sector composed of arc meander coil and iron-nickel alloy belt. The arc meander coil consists of several arc coils which connected to lateral coils in two ends alternately. It usually contains 4 to 9 arc elements which act as the main parts to generate the guided wave. In order to be bonded to the pipe, the arc meander coil is made by Flexible Printed Circuit Board. The iron-nickel alloy belt under the arc meander coil is like a ring and keeps consistent with the meander coil in size. It is pre-magnetizated in the circumferential direction and provides the static magnetic field.

There are two significant parameters in the design of the transducer: the central angle θ and the central radius r_c. θ and r_c correspond to the angle of arc coils and radius of middle part of the arc coils, respectively.

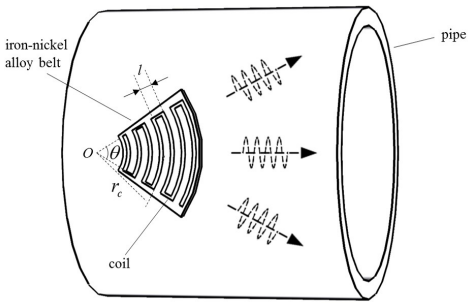

Fig. 2. Configuration of the proposed EMAT for MHSH waves

Denote r_1 and r_2 are the radius of arbitrary two adjacent arc coils respectively. Considering the MHSH wave generated by these two coils seperately, the phase of the particle vibration in any place r' can be expressed as:

$$\varphi_1 = \frac{2\pi(r' - r_1)}{\lambda} - \omega t + \varphi_{10} \tag{4}$$

$$\varphi_2 = \frac{2\pi(r' - r_2)}{\lambda} - \omega t + \varphi_{20} \tag{5}$$

where, λ is the wavelength, φ_{10} and φ_{20} is the initial phase of the waves. The special contra-flexure construction determines that the current in the adjacent arc coils is in the opposite direction and the initial phases satisfy:

$$\varphi_{10} - \varphi_{20} = \pm\pi \tag{6}$$

If the phase difference $\Delta\varphi = \varphi_1 - \varphi_2$ satisfies Eq.(7), the vibrations are superposed on each other and the amplitudes are enhanced, which promote the transduction efficiency.

$$\Delta\varphi = 2n\pi \quad (n = 1, 2, 3, \cdots) \tag{7}$$

Then the distance between the two adjacent arc coils along the radial direction, $l = r_2 - r_1$, should be

$$l = (2n \pm 1)\frac{\lambda}{2} \quad (n = 1, 2, 3, \cdots) \tag{8}$$

In other ways, this configuration can help generate single guided wave mode. The higher modes are weakened because their wavelengths do not satisfy the above rules.

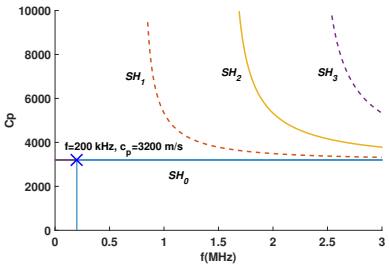

Fig. 3. Dispersion curve of SH wave

Specifically, the dispersion curve is referenced to select the wave mode. Fig.3 illustrates the dispersion curves of SH waves for a 2 mm thick steel plate. The velocity of longitudinal and transverse wave is 5400 m/s and 3200 m/s. From the dispersion curve, the phase velocity of SH_0 mode do not change with the frequency and remains 3200 m/s, which is advantageous in data processing. To avoid the higher modes, the working frequency is selected as 200 kHz. The corresponding wavelength is $\lambda = 16mm$.

IV. Numerical Analysis of the EMAT

A. Complete Magnetostrictive Model

The magnetostrictive effect can be described by the magnetostrictive curve obtained by experiments. It presents the relationship between the strain of the ferromagnetic material and the applied magnetic field. The magnetostrictive effect can be linearly approximated under a small dynamic magnetic field. It can be expressed as a linear piezomagnetic equation:

$$\begin{cases} \varepsilon = s\sigma + dH \\ B = d\sigma + \mu H \end{cases} \tag{9}$$

where, ε is strain tensor, σ is the stress tensor, H is the magnetic field strength, B is the magnetic flux density, s is the elastic compliance, μ is the permeability and d is the piezomagnetic coupling matrix.

The strain caused by magnetostrictive effect is

$$s_{MS} = dH_D \tag{10}$$

where, $H_D = [H_x; H_y; H_z]$ is the dynamic magnetic field strength caused by excitation current. Considering the transduciton of guided wave in two-dimensional plane strain and the dynamic magnetic field is perpendicular to the static magnetic field, the piezomagnetic coupling matrix becomes $d = [d_{11} \quad 0 \quad 0; d_{12} \quad 0 \quad 0; 0 \quad d_{35} \quad 0]$.

Then, the strain can be modeled using the equivalent source method [14]. According to the relation between stress and strain, the stress writing in component form is:

$$\begin{aligned} \sigma_{xx} &= \frac{Ed_{11}(2-\upsilon)}{2(1-\upsilon^2)} H_x \\ \sigma_{yy} &= \frac{Ed_{11}(2\upsilon-1)}{2(1-\upsilon^2)} H_y \\ \sigma_{xy} &= \frac{Ed_{35}}{2(1+\upsilon)} H_y \end{aligned} \tag{11}$$

where, E is Young's modulus, υ is Poisson's ratio. Furtherly, the traction vector, T, is the force vector on a cross-section divided by the its area. The relationship between the traction vector and stress at a point shown in Fig.4 meets the following equation:

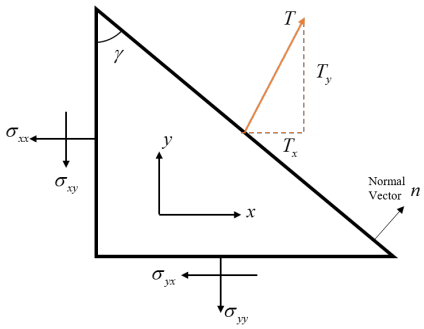

Fig. 4. Traction vector and stress

$$\begin{aligned} T_x &= \sigma_{xx}\cos\gamma + \sigma_{yx}\sin\gamma \\ T_y &= \sigma_{xy}\cos\gamma + \sigma_{yy}\sin\gamma \end{aligned} \tag{12}$$

where, γ is the angle between the normal vector of the element boundary and the horizontal axis of the coordinate. Therefore, stress can be equivalent to traction on the boundary under the condition that the stress state remains consistent everywhere. Then we get

$$\begin{aligned} T_x =& \frac{E}{2(1-\upsilon^2)}[H_x d_{11}(2-\upsilon)\cos\gamma \\ &+ H_y d_{35}(1-\upsilon)\sin\gamma] \\ T_y =& \frac{E}{2(1-\upsilon^2)}[H_y d_{35}(1-\upsilon)\cos\gamma \\ &+ H_x d_{11}(2\upsilon-1)\sin\gamma] \end{aligned} \tag{13}$$

Under the force load, elastic deformation occurs in the ferromagnetic object. Finally, the guided wave is generated and propagates along the object.

In the process of guided wave reception, the particle vibrates under the guided wave receiver. It produces dynamic magnetic field by the inverse magnetostrictive effect. Then the voltage is induced in the receiving arc meander coil. According to the knowledge of elastic dynamics, the isotropic ferromagnetic material satisfies the equation:

$$\rho\frac{\partial^2 \mathbf{u}}{\partial t} - \Delta \cdot \ \sigma = T \tag{14}$$

where, ρ is the density of material and $\mathbf{u}$ is the displacement vector. We can get strain ε by derivating the displacement $\mathbf{u}$. Combined with the strain-stress relation, it comes to stress σ.

According to Eq.(9) which indicate the inverse magnetostrictive effect, we can obtain the dynamic magnetic field through

$$B_D = d\sigma \tag{15}$$

Then the electromagnetic induction law can be used to obtain the induced electromotive force in the coil. Thus the complete magnetostrictive model including the guided wave excitation and reception is established.

B. Finite Element Modeling

The finite element method is applied to analyze the stress, strain and displacement of MHSH waves in pipe. To realize the simulation, the commercial finite element software Comsol Multiphysics is used. Comsol Multiphysics provides a solution for multi-physics modeling and is suitable for solving multi-physics coupling problems. The software modules used in EMAT contain AC/DC modules and Structural Mechanics Modules.

The modeling process includes: establishing the geometric model, setting the initial conditions and boundary conditions of the physical field, meshing, solving and post-processing. Some parameters of the EMAT for the MHSH waves is shown in Table I. In the AC/DC modules, the excitation current flows through the meander coil and excites the magnetic field in the air, the iron-nickel alloy belt and the pipe. In the Structural Mechanics Modules, the two end faces of the pipe are set as low reflection boundaries to minimize the effect of the reflection waves on the received signal. To ensure the accuracy of the simulation results and decrease the amount of calculation, the size of mesh in FEM follows the principle: $\Delta(x) \leq \frac{\lambda}{10}$. For observing the propagation of MHSH waves, the time transient analysis is used. The simulation time step is selected as $\Delta(t) \leq \frac{\Delta(x)}{c_L}$, where c_L is the velocity of longitudinal wave.

TABLE I
PARAMETERS OF IRON-NICKEL ALLOY BELT AND PIPE

Objects	**Young's modulus** ($\mathrm{P_a}$)	**Poisson's ratio**	**Density** ($\mathrm{k_g \cdot m^{-3}}$)	**Relative permeability**
Iron-nickel alloy belt	$207 \times e^9$	0.31	8880	250
Pipe	$205 \times e^9$	0.28	7850	150

The transducer is excited by tone burst current, which is a 5 cycle sine wave modulated with a Hamming window. The magnetic field simulation proves that the magnetic field is concentrated in the annular strip areas of the iron-nickel alloy belt under the arc coils. Therefore, the stress is concentrated and nearly even distributed in the annular strip areas. According to the magnetostrictive model, the stress can be equivalent to the traction along the boundary of the annular strip areas. Because of the traction, the ultrasonic wave is generated in pipe.

C. Radiation Pattern Analysis

The meander coil has an arc structure which can generate the MHSH waves in a certain range of angles. As shown in Fig. 5, the transducer generates MHSH waves which propagate forward at their respective angles. Due to the presence of multiple angularly transmitted guided waves in the detection area, the pipe is covered with a higher density of ultrasonic waves. A higher imaging resolution can be achieved using MHSH waves compared with that using the L or T mode, which propagates forward in the straight line.

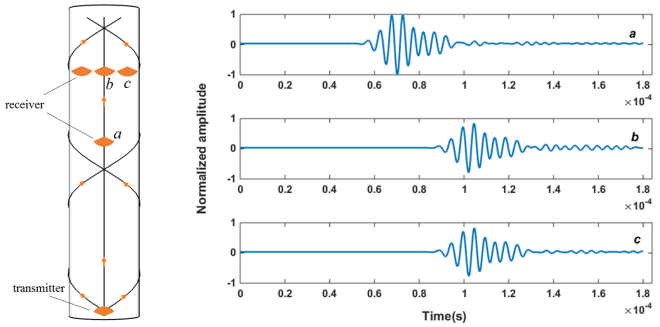

Fig. 5. The propagation of MHSH waves in pipe

First, the time of flight (TOF) of the wave packet is extracted to identity the wave mode. The group velocity (c_g) can be estimated as propagation distance divided by the TOF. Choose point a and point b as the observation point shown in Fig.5 and calculate the velocity of wave propagation. The error between the simulative group velocity $c_{gs} = 3061$m/s and theoretical group velocity $c_{g'}$ of 3200 m/s is: $error = \frac{|c_{gs} - c_{g'}|}{c_{g'}} = 4.34\%$. The velocity from point a to point c is also measured and the result is consistent with the theoretical one. This proves that the MHSH waves are generated correctly.

Second, study the radiation pattern of MHSH waves. The transmitter is arranged on one side of the pipe and several receiver is arranged evenly in the circumferential direction on the other side of the pipe. The annulus section of pipe end is set as the low reflection boundary, therefore, the reflection signal from the end of pipe can be avoided. This approach also decreases the consumption of simulation time and memory usage. The received signal is normalized to the range of 0 to 1, shown in Fig.6. It clearly shows that the ultrasonic wave beam is concentrated in a certain range of angle and the energy attenuates quickly in other angles. This means that the transducer can generate HSH wave in multi-angles.

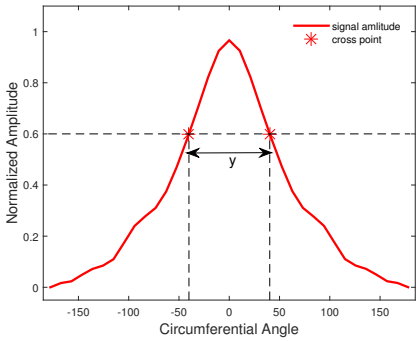

Fig. 6. Beam divergence angle

Then, we define the beam divergence angle α . As Fig.6 shows, the horizontal dashed line is the 60% attenuation line whose amplitude is 60% of the maximum amplitude. The cross point is the 60% attenuation point. The angle between the two lines which connect the two attenuation points and the

transmitter point is referred as the beam divergence angle. It expresses as Eq.(16). The greater α means the more disperse energy and the larger helical angles.

$$\alpha = 2arctan(\frac{\frac{y}{2}}{l}) \tag{16}$$

In next part, the influences of the parameters to the beam divergence angle are discussed in both simulations and experiments.

V. Experimental Verification

In this part, several experiments are performed on a steel pipe to verify the effectiveness of the proposed transduer for MHSH waves. Meanwhile, relevant simulations and experiments are conducted to test the circumferential distribution of received signals and analyze the influence of two structure parameters of the transducer.

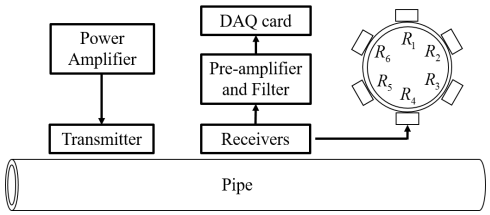

Fig. 7. Schematic diagram of the experimental system

Fig.7 shows the schematic diagram of the experimental system. The outer diameter and wall thickness of the pipe are 219 mm and 6 mm, respectively. One transmitter is installed on the left side and six receivers placing evenly around the pipe are installed on the right side. The voltage of the excitation signal from the power amplifier RITEC RPR-4000 is approximately 300 V. The frequency is 200 kHz and the periodicity is 5 as in the simulation. The signals from the receivers are amplified and filtered by the signal conditioning circuit. The central frequency and bandwidth of the filter are 200 kHz and 20 kHz, respectively. Finally the data is collected and sent to the PC to be analyzed.

First, same as the process of the simulation in above part, the wave mode is verified by comparing the theoretical and experimental velocity. The direct distance between the two observation points is 100 mm. Then TOF of the wave packet is extracted to obtain the group velocity. The error between the experimental velocity $c_{ge} = 3126$ m/s and theoretical $c_{g'}$ of 3200 m/s is: $error = 2.3\%$.

Second, simulations and experiments to verify the the circumferential distribution of received signals are conducted. Different parameters of the transducer are taking into account.

Step 1, change the central angle θ of the transducer and collect the received signal. In the experiments, six identical receivers same with the transmitter but in a distance of 200 mm away are adopted. The results are plotted in Fig.8. It is clear that the results of experiments keep consistent with those of simulations. The energy concentrates in a certain range of angles and the waves propagate in both straight and

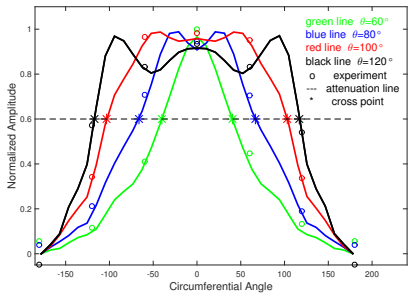

Fig. 8. Results of different central angles

helical directions. To evaluate the performance of transducer for MHSH waves, the beam divergence angle α defined in last part is calculated and presented in Fig.9.

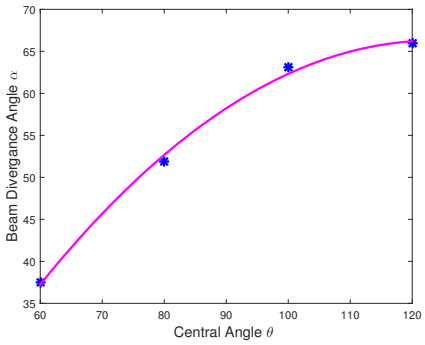

Fig. 9. The beam divergence angle and central angle

The beam divergence angle is approximately half of the central angle and increases non-linearly with the central angle. By using the polynomial fitting method, we can obtain the quadratic relationship between α and θ as in Eq.(17). This equation can be applied to predict the beam divergence angle if the central angle is known.

$$\alpha = -0.0072\theta^2 + 1.7819\theta - 43.674 \tag{17}$$

Step 2, change the central radius r_c and observe the variance of the beam divergence angle. The simulations match the experiments in the circumferential distribution of received signal. Here we only give the beam divergence angles under different central radii, which are presented in Table II.

TABLE II
Beam Divergence Angles of Different Central Radii

Central radius(mm)	30	40	50	60
Beam divergence angle(°)	37.3	43.3	43.9	44.7

It clearly shows that with a larger central radius, the beam divergence angle becomes larger but in a non-linear way. Compare the effects of central angle and central radius, both parameters influence the distribution of the received signals,

however, the central angle brings more significant change to beam divergence angle. Therefore, the central angle is the main factor and the first consideration when designing transducers for MHSH waves.

VI. Conclusions

This work proposes a new EMAT for MHSH waves. This EMAT is composed of iron-nickel alloy belt and arc meander coil. It overcomes the disadvantages of the narrow beam directivity and disperse energy of present transducers, and the generated guided wave could cover the region of detection with fewer EMATs. This EMAT is analyzed by numerical simulations and confirmed by experiments. Furthermore, the influences of two structure parameters on the beam divergence angle are studied and the results indicate that the central angle is the first consideration when designing the new transducers for MHSH waves. This new EMAT might have potentials in providing an efficient solution for pipe inspection.

Acknowledgment

This research was financially supported by the National Natural Science Foundation of China (grant No. 51677093 and No. 51777100).

References

[1] H. Kwun and A. E. Holt, "Feasibility of under-lagging corrosion detection in steel pipe using the magnetostrictive sensor technique," *Ndt & E International*, vol. 28, no. 4, pp. 211–214, 1995.

[2] A. Demma, P. Cawley, M. Lowe, A. G. Roosenbrand, and B. Pavlakovic, "The reflection of guided waves from notches in pipes: a guide for interpreting corrosion measurements," *NDT & E International*, vol. 37, no. 3, pp. 167–180, 2004.

[3] H. Kuansheng, H. Songling, Z. Wei, W. Zheng, W. Shen, and H. Zijing, "A new frequency-tuned longitudinal wave transducer for nondestructive inspection of pipes based on magnetostrictive effect," *Sensors Applications Symposium IEEE*, pp. 64 – 68, 2010.

[4] D. Zhang, Z. Zhou, J. Sun, E. Zhang, Y. Yang, and M. Zhao, "A magnetostrictive guided-wave nondestructive testing method with multifrequency excitation pulse signal," *IEEE Transactions on Instrumentation and Measurement*, vol. 63, no. 12, pp. 3058–3066, 2014.

[5] J. S. Lee, Y. Y. Kim, and S. H. Cho, "Beam-focused shear-horizontal wave generation in a plate by a circular magnetostrictive patch transducer employing a planar solenoid array," *Smart Materials and Structures*, vol. 18, no. 1, p. 015009, 2009.

[6] Z. Wei, S. Huang, S. Wang, and W. Zhao, "Magnetostriction-based omni-directional guided wave transducer for high-accuracy tomography of steel plate defects," *IEEE Sensors Journal*, vol. 15, no. 11, pp. 6549–6558, 2015.

[7] M. Hirao and H. Ogi, "An SH-wave EMAT technique for gas pipeline inspection," *NDT & E International*, vol. 32, no. 3, pp. 127–132, 1999.

[8] X. Zhao and J. L. Rose, "Guided circumferential shear horizontal waves in an isotropic hollow cylinder," *Journal of the Acoustical Society of America*, vol. 115, no. 5, pp. 1912–1916, 2004.

[9] W. Luo, J. L. Rose, and H. Kwun, "Circumferential shear horizontal wave axial-crack sizing in pipes," *Research in Nondestructive Evaluation*, vol. 15, no. 4, pp. 149–171, 2005.

[10] S. Wang, S. Huang, W. Zhao, and Z. Wei, "3D modeling of circumferential SH guided waves in pipeline for axial cracking detection in ILI tools," *Ultrasonics*, vol. 56, pp. 325–331, 2015.

[11] H. W. Kim, J. K. Lee, and Y. Y. Kim, "Shear-horizontal wave-based pipe damage inspection by arrays of segmented magnetostrictive patches," *IEEE Transactions on Ultrasonics Ferroelectrics and Frequency Control*, 2011.

[12] H. W. Kim, H. J. Lee, and Y. Y. Kim, "Health monitoring of axially-cracked pipes by using helically propagating shear-horizontal waves," *NDT & E International*, vol. 46, pp. 115–121, 2012.

[13] J. Li and J. L. Rose, "Natural beam focusing of non-axisymmetric guided waves in large-diameter pipes," *Ultrasonics*, vol. 44, no. 1, pp. 35–45, 2006.

[14] H. J. Kim, J. S. Lee, H. W. Kim, H. S. Lee, and Y. Y. Kim, "Numerical simulation of guided waves using equivalent source model of magnetostrictive patch transducers," *Smart Materials and Structures*, vol. 24, no. 1, p. 015006, 2014.